



Surprising Effects of Synaptic Excitation*

JONATHAN E. RUBIN

*Department of Mathematics and Center for the Neural Basis of Cognition,
University of Pittsburgh, Pittsburgh, PA 15260*

rubin@math.pitt.edu

Received November 30, 2004; Revised January 7, 2005; Accepted January 13, 2005

Abstract. Typically, excitatory synaptic coupling is thought of as an influence that accelerates and propagates firing in neuronal networks. This paper reviews recent results explaining how, contrary to these expectations, the presence of excitatory synaptic coupling can drastically slow oscillations in a network and how localized, sustained activity can arise in a network with purely excitatory coupling, without sustained inputs. These two effects stem from interactions of excitatory coupling with two different forms of intrinsic neuronal dynamics, and both serve to highlight the fact that the influence of synaptic coupling in a network depends strongly on the intrinsic properties of cells in the network.

Keywords: synaptic excitation, firing frequency, delayed escape, way-in way-out function, canard, localized activity, go surface

1. Introduction

A fact that is well known in the computational neuroscience community, but important enough to re-emphasize here, is that synaptic coupling has far different implications than diffusive coupling for pattern formation. Synaptic coupling, driven by neurotransmitters, can act over a variety of timescales, possibly after some initial delay, and neurotransmitters' effects may far outlast the events that elicit their release (e.g., Abbott and Regehr, 2004). Further, synaptic coupling is generally non-local, with a broad range of spatial connection patterns observed across different neuronal systems. These features allow synapses to influence the dynamics of neuronal networks in a wide variety of ways, many of which are complex to analyze.

To gauge the effects of synaptic coupling on the dynamics of a network with a given coupling architecture, it is natural to consider the behavior of the network with all coupling blocked and then to ask how the in-

roduction of synaptic coupling changes the activity of the cells in the network. Of course, the answer to this question depends on how strong a coupling is introduced, which can be made precise by specifying a value for the maximal synaptic conductance or weight associated with each synapse. The effects induced on any subset of cells within a network by the introduction of synaptic coupling can be broadly classified as effects on firing rates alone versus effects on firing patterns. Examples of the latter include changes in synchrony, more general changes in the temporal relations of firing times, and switches between modes of activity such as silence, bursting, and tonic spiking.

Many particular examples of the effects of synaptic coupling have been elucidated theoretically, some of which are intuitive and some less so, some considered in the context of models for particular neuronal networks and some in abstract models. A full review of computational work on pattern formation driven by synaptic coupling in neuronal networks would require volumes. In this article, I will review some specific, recent results on surprising effects that can be induced by *excitatory* synaptic coupling, which is generally

*This work was partially supported by the National Science Foundation, under award DMS-0414023.

expected to accelerate and promote firing. The first finding that I will discuss is that synaptic excitation, particularly with a slow decay constant, can yield a drastic slowing of tonic spiking or burst firing in certain types of networks (Drover et al., 2005), typified by a network of classical Hodgkin-Huxley neurons (Hodgkin and Huxley, 1952). The mechanism underlying this slowing relates to *canards*, which are solutions to systems of differential equations that spend a prolonged time near structures that are unstable in the corresponding phase space (Diener, 1984; Szmolyan and Wechselberger, 2001). The second result that I will present is that a network of intrinsically silent cells, with distance-dependent excitatory synaptic coupling and *no inhibitory coupling*, can support sustained, localized activity in the absence of sustained external input (Rubin and Bose, 2004). The existence of such solutions requires a mechanism by which the network dynamics generates spatial variations in the level of synaptic excitation, such that there is enough excitation available to maintain activity in one area but not enough to recruit cells from other areas, despite the fact that the coupling architecture is spatially homogeneous. Taken together, these results highlight the fact that cells' intrinsic dynamics can be crucial in determining the activity patterns that arise when synaptic coupling between the cells is introduced.

2. Basics of Dynamic Synaptic Excitation

A wide variety of conventions have been used to model neurons and synapses in computational analyses of neuronal networks. Let us consider ordinary differential equation representations of single neurons, which under the inclusion of synaptic coupling become

$$\begin{aligned} v' &= f(v, w) + I_{\text{syn}} \\ w' &= g(v, w), \end{aligned} \quad (1)$$

where v denotes some measure of the activity or excitability of the cell, $'$ denotes differentiation with respect to time t , w is a vector of auxiliary variables, and I_{syn} corresponds to some measure of synaptic input. For concreteness, the remainder of this discussion focuses on the case where v in Eq. (1) denotes the voltage across the cell membrane, such as in the Hodgkin-Huxley (HH) or conductance-based formalism, although similar concepts apply in other models. In this case, I_{syn} is the total synaptic current to the cell, and both terms in the right hand side of the v -

equation incorporate scaling by the reciprocal of the membrane capacitance, henceforth normalized to 1 and omitted.

Commonly,

$$I_{\text{syn}} = - \sum_j w_j \left[\sum_i \alpha(t - t_j^i) \right] (v - v_{\text{syn}_j}),$$

where w_j denotes a synaptic weight from cell j , t_j^i is the firing time of spike i of cell j , the synaptic reversal potential v_{syn_j} is a parameter determined by the type of input sent by cell j , and the α -function $\alpha(t)$ takes the form $t^n e^{-kt} H(t)$ where n is a small nonnegative integer, $k > 0$ is a parameter, and $H(t)$ is the Heaviside step function. Richer effects can be observed, however, by considering dynamic synapses, which we represent here by

$$I_{\text{syn}} = - \sum_j g_j s_j (v - v_{\text{syn}_j}), \quad (2)$$

where $g_j \geq 0$ denotes the maximal synaptic conductance from cell j and s_j satisfies its own differential equation, typically of the form

$$s_j' = a(v_j)(1 - s_j) - b s_j. \quad (3)$$

Here, $a(v)$ is an increasing sigmoidal function taking nonnegative values, such that when the voltage v_j of cell j crosses some threshold, s_j grows, while s_j decays when v_j is below that threshold, with s_j constrained by its dynamics to lie in $[0, 1]$ for all time. Clearly, such dynamic synapses allow for highly variable time courses of synaptic input, unlike α -functions, with these time courses shaped by presynaptic cells' activity patterns.

From Eq. (2), given that $g_j s_j \geq 0$ for all j , it follows that the sign of each term in I_{syn} is opposite to that of $v - v_{\text{syn}_j}$. If, for some j , $v - v_{\text{syn}_j} > 0$ over most physiologically relevant v values, then the synaptic input modelled by the j term in I_{syn} is called *inhibitory*. Similarly, *excitatory* synaptic inputs are roughly defined as those for which $v - v_{\text{syn}_j} < 0$ over most relevant values of v . Based on this definition, it is clear from Eqs. (1) and (2) that excitatory inputs tend to make v' more positive. This leads to a natural expectation that excitatory inputs will tend to depolarize cells, promoting or accelerating action potential generation. It is known, however, that depolarization does not always lead to enhanced spiking; in depolarization block, for example, a neuron achieves a stable steady state in which its membrane potential is quite elevated yet its spike-generated currents are inactivated and spiking is

eliminated. In the next section, I will discuss some examples where firing persists but slows in the presence of synaptic excitation and will in particular examine a recently elucidated, dynamically more complex mechanism through which synaptic excitation can drastically retard firing, without shutting it down completely.

Before moving to this topic, however, it is important to note that synaptic inputs can influence the activity pattern across a network of cells, not just firing rates. A large number of previous papers have shown that whether the synapses in a network are excitatory or inhibitory has a dramatic impact on the stability of synchrony within the network. From an intuitive point of view, it is not unreasonable to expect that synaptic excitation would promote synchrony: if a cell that fires sends synaptic excitation to another cell, then this should push the other cell to fire as well, tending to synchronize the cells. An earlier surprise in the study of synaptic excitation was that its actual impact on synchrony is much more subtle and in fact depends crucially on the intrinsic dynamics of the cells in the network (the $f(v, w)$ and $g(v, w)$ in Eq. (1)) (Ermentrout, 1996; Hansel et al., 1995; Somers and Kopell, 1993), with co-existence of stable in-phase and anti-phase solutions even possible (Kopell and Somers, 1995).

3. Low-Frequency Synchronized Firing with Synaptic Excitation

Previous computational work has shown that synaptic excitation can diminish the firing frequency of mutually coupled cells. In the case of a network of identical Hodgkin-Huxley (HH) neurons with all-to-all coupling by α -function synapses, Hansel et al. (1993) found such a drop in firing rate, from an uncoupled rate of about 68 Hz down to frequencies of just above 50 Hz, under the assumption of weak coupling. The weak coupling assumption entails supposing that all neurons evolve on limit cycles and that the effect of each synaptic input will only be felt during a single excursion around the cycle (Hoppensteadt and Izhikevich, 1997). Given this framework, the effects of an excitatory synaptic input can be expressed as a change in phase relative to the unperturbed case, encoded in a phase resetting curve (PRC). The results obtained in Hansel et al. (1993) depend on the fact that the network considered consists of so-called type II neurons (see e.g. Hansel et al., 1995), which have negative regions in their PRCs.

Strong synaptic excitation has also been observed to slow oscillations in a quite different setting, namely

in relaxation oscillators coupled with strong dynamic synapses of the form (2), (3) (Kopell and Somers, 1995; Butera et al., 1999). Relaxation oscillators are used to model the burst envelopes of cells firing bursts of spikes. In terms of Eq. (1), with w scalar for simplicity, a relaxation oscillator can be obtained by assuming that $g(v, w) = \epsilon g_1(v, w)$ for $0 < \epsilon \ll 1$, that the v -nullcline $\mathcal{N}_V = \{(v, w) : v' = 0\}$ can be expressed as the graph of a cubic function $w = N_f(v)$ (see Fig. 1), and that the w -nullcline $\mathcal{N}_W = \{(v, w) : w' = 0\}$ and \mathcal{N}_V intersect only along the middle branch of \mathcal{N}_V , corresponding to an unstable critical point of (1). Under these conditions, the v -dynamics will quickly drive trajectories of (1) into a small neighborhood of \mathcal{N}_V , where the w -dynamics will dictate the direction and speed of evolution. Trajectories will jump between the branches of \mathcal{N}_V at its local extrema, yielding the oscillation in Fig. 1A. We will refer to those times when the oscillator is near the right (left) branch of \mathcal{N}_V as the oscillator's active (silent) phase.

Let $s = \sum_j g_j s_j$ denote the total synaptic conductance to a cell, and assume that v_{syn_j} in Eq. (2) is independent of j , corresponding to the case that all inputs to

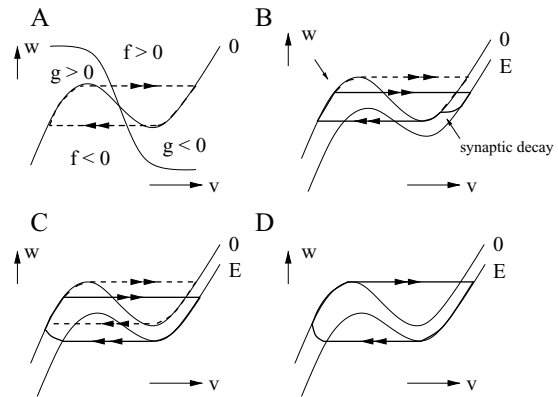


Figure 1. Nullclines for a relaxation oscillator. The cubic curves labelled with 0 represent $\mathcal{N}_V(0)$, with $f > 0$ ($f < 0$) above (below) the curve, while those labelled with E represent $\mathcal{N}_V(s)$ for some maximal $s > 0$. (A) The sigmoidal curve denotes \mathcal{N}_W , with $g > 0$ ($g < 0$) below (above) the curve. The dashed curve, marked with arrows on fast jumps between branches of $\mathcal{N}_V(0)$, is a periodic solution called a relaxation oscillation. (B) The baseline relaxation oscillation (dashed) is modulated by an excitatory synaptic input with very fast onset (received when the cell lies at the location marked by the upper left arrow), which wears off while the cell is in the active phase (lower right arrow), shortening the oscillation (solid). (C) An input of longer duration extends the active phase. (D) Two synchronized cells send each other synaptic excitation, and thus follow the E curve, while they are in the active phase. Synaptic excitation decays, and the cells return the 0 curve, in the silent phase. The period of oscillation has been increased relative to (A).

a cell are of the same type. Due to the I_{syn} term in (1), the v -nullcline is actually parametrized by s , and we henceforth denote it by $\mathcal{N}_V(s)$ correspondingly. In Fig. 1B–D, $\mathcal{N}_V(0)$ is labelled with 0. Since $I_{\text{syn}} > 0$, increasing s from 0 moves $\mathcal{N}_V(s)$ into regions where $f(v, w) < 0$, which leads to a lowering of $\mathcal{N}_V(s)$ as s increases. Through this lowering effect, an excitatory synaptic input with rapid onset can speed up the entry into the active phase of the cell that receives it (the postsynaptic cell), as shown in Fig. 1B. Now, if the cell that provided the input (the presynaptic cell) leaves the active phase, then the synaptic input to the postsynaptic cell begins to decay, as in Fig. 1B, and the overall oscillation of the postsynaptic cell encompasses a smaller extent in phase space, typically corresponding to a shorter time duration. Alternatively, if the cells are close to synchrony, then the presynaptic cell will remain active along with the postsynaptic cell, and thus the synaptic input will remain elevated. This can prolong the active phase of the postsynaptic cell, as shown in Fig. 1C, such that overall, synaptic excitation may shorten or prolong the oscillation period. Finally, if the cells are reciprocally connected by synaptic excitation and synchronize, as is possible for relaxation oscillators (Somers and Kopell, 1993), then they can together experience prolonged oscillations, relative to the uncoupled case, as shown in Fig. 1D.

In contrast to the weak coupling case, where the delay is induced by the onset of excitation and is of limited magnitude, and the relaxation oscillator case, where the delay results from an extended active phase,

Fig. 2A shows the time course of the membrane potential of an HH neuron, reduced to a system of two intrinsic equations (Rinzel, 1985) and coupled to itself with synaptic excitation. The equations simulated here, using XPPAUT (Runge-Kutta with $dt = 0.05$ msec in this example) (Ermentrout, 2002), are

$$\begin{aligned} cv' &= -g_L(v - v_L) - g_K n^4(h)(v - v_K) \\ &\quad - g_{\text{Na}} m_\infty^3(v) h(v - v_{\text{Na}}) + I - g_{\text{syn}} s(v - v_{\text{syn}}) \\ h' &= (h_\infty(v) - h)/\tau_h(v) \\ s' &= a(v)(1 - s) - s/\tau_{\text{syn}} \end{aligned} \quad (4)$$

with $n(h) = \max(.801 - 1.03h, 0)$, with $x_\infty(v) = \alpha_x(v)/(\alpha_x(v) + \beta_x(v))$ for $x = m$ or h , and with $\alpha_h(v) = .07 \exp(-(v + 65)/20)$, $\beta_h(v) = 1/(1 + \exp(-(v + 35)/10))$, $\alpha_m(v) = 0.1(v + 40)/(1 - \exp(-(v + 40)/10))$, $\beta_m(v) = 4 \exp(-(v + 65)/18)$, $a(v) = 2/(1 + \exp(-v/5))$. Parameter values are taken to be $v_{\text{Na}} = 50$, $v_K = -77$, $v_L = -54.4$, $g_{\text{Na}} = 120$, $g_K = 36$, $g_L = 0.3$, $c = 1$, $I = 13$, and $v_{\text{syn}} = 0$, with units of mV for voltages, mS/cm² for conductances, and $\mu\text{A}/\text{cm}^2$ for current. In the simulation, $\tau_{\text{syn}} = 5$ msec and the maximal synaptic conductance g_{syn} begins at zero; when this is instantaneously switched up to 2, the oscillation frequency drastically slows. Much more extreme slowing can be achieved by increasing τ_{syn} , and similar slowing occurs in response to the introduction of synaptic excitation into a network of all-to-all coupled HH cells. The mechanism underlying the slowing shown here entails an extreme extension of the silent

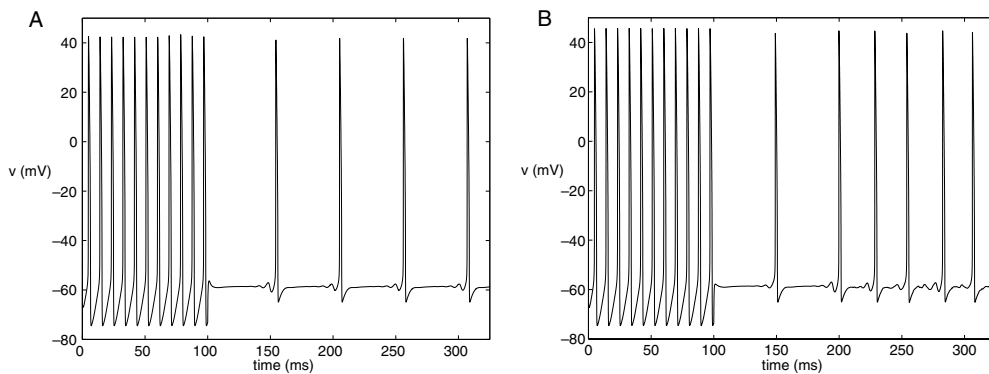


Figure 2. (A) The firing of a reduced, self-coupled HH model neuron is drastically slowed by synaptic excitation, which is introduced after 100 msec. (B) The same experiment shown in (A) is simulated but with Gaussian white noise introduced additionally into the v and h equations of system (4), starting at 200 msec. Due to noise, firing frequency slightly increases but the cell's activity remains qualitatively similar to the deterministic case, with significant slowing maintained.

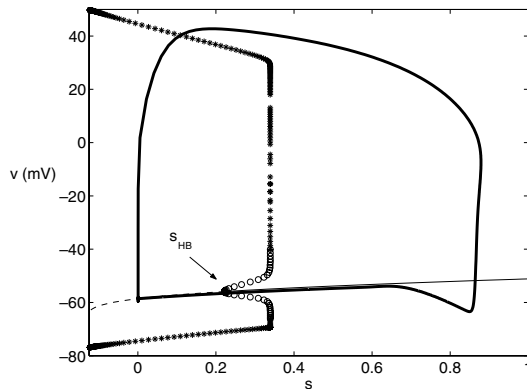


Figure 3. The bifurcation diagram for (4) with s taken as a bifurcation parameter, with a trajectory of (4) superimposed. The thin curve across the lower portion of the plot, near $v = -60$ mV, is a curve of equilibria, $\mathcal{N}_V(s) \cap \mathcal{N}_H$. These points destabilize in a subcritical Hopf bifurcation as s decreases through s_{HB} . In this bifurcation, a family of unstable periodic orbits appears; the open circles here denote the maximal and minimal v -values along these orbits. This family coalesces in a saddle-node bifurcation with a larger amplitude family of stable periodic orbits, denoted here by asterisks, as s increases. The thicker solid curve is a trajectory of (4), which illustrates the delay in escape from the branch of equilibria until s decays to values well below s_{HB} .

phase between spikes, during which time the synaptic input decays, quite unlike the weak coupling and relaxation oscillator scenarios.

In keeping with convention, in system (4), the intrinsic variables are (v, h) , rather than (v, w) . It can be shown that for each fixed s , the nullclines $\mathcal{N}_V(s)$ and \mathcal{N}_H intersect in a single point, which corresponds to a critical point for the (v, h) equations of (4). Indeed, Fig. 3 shows the bifurcation diagram for this pair of equations, with s taken as a bifurcation parameter. The form of this bifurcation diagram, in which the critical point destabilizes through a subcritical Hopf bifurcation as s decreases, corresponding to the decay of synaptic excitation, suggests that the retardation of firing may result from a *delayed escape* or *delayed bifurcation* phenomenon. In delayed escape, trajectories initially contract toward an attracting curve of equilibria for a fast subsystem. Here, the (v, h) equations from (4) would play the role of the fast subsystem, with the contraction strength quantified by the real parts of the eigenvalues of the linearization of the system $(dv/ds, dh/ds)$, derived from (4), about this curve. Eventually, the $O(\epsilon)$ drift of a slow variable (here s) pulls trajectories through a subcritical Hopf bifurcation that destabilizes the equilibrium curve with respect to the fast subsystem. The trajectories continue

to remain in an $O(\epsilon)$ neighborhood of the now repelling equilibrium curve for an $O(1/\epsilon)$ time, however, until the expansion governed by the now positive real parts of the eigenvalues of the linearization accumulates sufficiently to counter the earlier contraction. The time needed to escape from this curve can be calculated using a *way-in way-out function* (Diener, 1984; Neishtadt, 1987, 1988). Interestingly, this delayed escape effect gives rise to elliptic bursting (Rinzel, 1987; Wang and Rinzel, 1995; Hoppensteadt and Izhikevich, 1997; Rubin and Terman, 2002) when the drift direction of the slow variable switches after escape and the periodic orbits born from the Hopf bifurcation have appropriate characteristics (Baer et al., 1989; Izhikevich, 2000; Kuske and Baer, 2002; Su et al., 2004).

Attributing the synaptically-induced slowing in system (4) to delayed escape leads to trouble, however. First, the rate of decay of s is comparable to the rate of evolution of h , violating the assumptions of the delayed escape theory. Further, if this problem is ignored and the way-in way-out function for (4) is calculated by treating s as a slow variable, the delay in escape is significantly underestimated (with an $O(1)$ error as $\tau_{\text{syn}} \rightarrow \infty$ under the assumption that $h' = \epsilon g(v, h)$ with $\epsilon \tau_{\text{syn}} = O(1)$) (Drover et al., 2005).

A more accurate explanation for the extreme slowing in the self-coupled HH neuron is presented in Drover et al. (2005). As we assumed earlier for relaxation oscillators, it turns out here that the equation $v' = 0$ for the v -nullcline $\mathcal{N}_V(s)$ can be solved to obtain a function $h = N_f(v, s)$, which has a unique local maximum, or left knee, at fairly hyperpolarized v and a unique local minimum at more depolarized v . The idea explained in Drover et al. (2005) is that the flow of (4) in the vicinity of the curve of left knees forms a vortex structure, the *vortex canard*, that traps trajectories. To understand the mechanism underlying the vortex, consider a solution $x(t) = (v(t), h(t), s(t))$ of (4), with $x(0) = (v_0, h_0, s_0)$ lying in a small neighborhood of $\mathcal{N}_V(s_0)$. As $x(t)$ evolves, we can compare the value of $h(t)$ to the evolving value of $N_f(v(t), s(t))$. In particular, the instantaneous change in the difference between these h -values is given by $H(t) := d(h(t) - N_f(v(t), s(t)))/dt$.

For an appropriate fixed s_0 , we can partition points (v, h, s_0) in the $\{s = s_0\}$ slice of (v, h, s) -phase space into those that initially “fall behind” $\mathcal{N}_V(s)$, corresponding to $H(0) < 0$, and those that “catch up” to $\mathcal{N}_V(s)$, corresponding to $H(0) > 0$, under (4). Denote the former set of points by $\tilde{A}(s)$. Close to the curve of

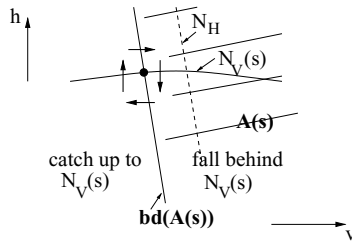


Figure 4. The vortex structure associated with (4) in the (v, h) plane, near the left knee of $\mathcal{N}_V(s)$, for fixed s . The region with solid lines across it is $A(s)$, which includes the h -nullcline \mathcal{N}_H (dashed line). The arrows illustrate the directions that representative trajectories will instantaneously move under (4), relative to $\mathcal{N}_V(s)$, as described in the text.

left knees, $\partial N_f(v, s)/\partial v$ is small relative to the rate of change of h , and $\tilde{A}(s)$ can be approximated for simplicity by

$$A(s) = \left\{ (v, h) : \frac{(h_\infty(v) - h)}{\tau_h(v)} < \frac{\partial N_f(v, s)}{\partial s} \frac{ds}{dt} \right\}, \tag{5}$$

where the term on the left side of the inequality in Eq. (5) comes from the h equation in (4). An illustration of this structure in the (v, h) plane is given in Fig. 4.

For each fixed $s \in [0, s_{\max}]$, where s_{\max} is the value of s at which a trajectory of interest enters a specified neighborhood of the curve of left knees, let $(\hat{v}(s), \hat{h}(s))$ denote $bd(A(s)) \cap \mathcal{N}_V(s)$. Further, let

$$A = \bigcup_{s=0}^{s=s_{\max}} A(s) \quad \text{and} \quad \mathcal{N}_V = \bigcup_{s=0}^{s=s_{\max}} \mathcal{N}_V(s).$$

Based on the above structure, it seems reasonable that trajectories that enter a neighborhood of the curve $(\hat{v}(s), \hat{h}(s), s)$ will spiral around $(\hat{v}(s), \hat{h}(s), s)$ during their time in the silent phase, in a vortex-like structure or vortex canard (Drover et al., 2005), under the flow of (4). More specifically, trajectories lying in A and below \mathcal{N}_V will be unable to cross through \mathcal{N}_V and will instead exit A through $bd(A)$, since $v' < 0$ below \mathcal{N}_V . Once outside of A , they will eventually cross through \mathcal{N}_V to enter the region where $v' > 0$. Before they can escape the neighborhood of $(\hat{v}(s), \hat{h}(s), s)$, however, they re-enter A and thus may fall below \mathcal{N}_V , such that $v' < 0$ once again. A projection of this motion onto the (v, h) plane is sketched in Fig. 4; see Drover et al. (2005) for further discussion.

While this analysis is not precise, with vagueness in selecting a neighborhood such that $\partial N_f(v, s)/\partial v$ is small, it suggests that the delay in escape can be estimated by computing a modified way-in way-out function. Unlike the standard way-in way-out calculation, which proceeds by linearizing $(dv/ds, dh/ds)$ about the intersection of $\mathcal{N}_V(s)$ with \mathcal{N}_H for each s , the modified way-in way-out function is derived from linearization about $(\hat{v}(s), \hat{h}(s))$ to capture the vortical structure there. In Drover et al. (2005), the modified way-in way-out function is shown to give an accurate estimate of the duration of delayed escape, and correspondingly of the s -value at which escape occurs, over a wide range of synaptic decay rates τ_{syn} . Further, it is demonstrated analytically that for $h' = \epsilon g(v, h)$ with $\epsilon \tau_{\text{syn}} = O(1)$, the error in the time calculation is $O(1/\tau_{\text{syn}})$, if $\partial N_f(v, s)/\partial v$ is small near $(\hat{v}(s), \hat{h}(s))$. Of course, as τ_{syn} grows for ϵ fixed, $|ds/dt|$ decreases and $bd(A(s))$ approaches \mathcal{N}_H for each s , such that the modified and standard way-in way-out calculations approach equivalence. Finally, the same delay effect can yield bursting solutions, in which multiple spikes are separated by prolonged interburst intervals. A short interspike interval can arise when the synaptic excitation s remains below the Hopf bifurcation value s_{HB} after an initial spike, such that no trapping in the silent phase results. A burst of spikes can follow as s gradually accumulates, with termination once $s > s_{\text{HB}}$ occurs (Drover et al., 2005).

Recently, Wechselberger (2004) has demonstrated that the extreme delay discussed here fits the criteria for a folded node canard in \mathbb{R}^3 (Szmolyan and Wechselberger, 2001). Thus, the ‘‘vortex structure’’ to which the trapping is ascribed in Drover et al. (2005) can be rigorously understood in terms of invariant manifolds of the full system (4), which form a multi-layered trapping region. A nice aspect of the manifold calculations, given for a FitzHugh-Nagumo model of the HH equations in Wechselberger (2004), is that they illustrate the robustness to noise of this delayed escape phenomenon. An example of this robustness is illustrated in Fig. 2B; more generally, simulations with $\tau_{\text{syn}} = 5$ ms yield a firing rate of 108.65 Hz without coupling, 19.68 Hz with $g_{\text{syn}} = 2$ mS/cm² and no noise, and 35.48 ± 0.92 Hz with $g_{\text{syn}} = 2$ mS/cm² and the same level of noise shown in Fig. 2B, and similar results arise for different τ_{syn} , g_{syn} , and I . While noise can push a trajectory across some layers of the trapping region, thereby hastening its escape from the silent phase, the outer layers still provide a trapping effect.

4. Sustained, Localized Activity in an Excitatory Network

Through its depolarizing effect, synaptic excitation pulls silent cells closer to spike threshold, possibly giving them an opportunity to fire. By this means, waves of activity can propagate through linear and two-dimensional networks with appropriately strong synaptic excitation, in some cases leaving all cells active in their wake, as has been detailed in many computational studies and some experimental work. While synaptic excitation can sustain spatially extended activity once it is initiated, the standard recipe for the spatial localization of activity has been so-called lateral inhibition or Mexican hat coupling. In Mexican hat coupling, cells are connected to nearby cells via excitation and to more distant cells via inhibition, which can act as a brake on the spread of activity; many of the works harnessing this idea draw inspiration from the Wilson and Cowan (1973) and Amari (1977) models.

Since in general a single neuron will release a single type of neurotransmitter, a biophysically realistic incarnation of Mexican hat coupling requires at least two cell populations, one excitatory (E) and one inhibitory (I). Sustained, localized activity, or bumps, can be achieved in a model network when the synapses from the E cells target nearby E and I cells, while synapses from the I cells to the E cells have a greater spatial extent. A variety of brain areas, including the thalamus and the indirect pathway of the basal ganglia, appear to lack E-to-E connections, however. Therefore, the question of whether alternative architectures can also support bumps arises. Recent work has shown that post-inhibitory rebound (PIR), a form of hyperpolarization-induced firing with delay, can replace E-to-E connections as a mechanism for sustaining activity (Rubin et al., 2001). And even in the absence of PIR, appropriately scaled E and I connection architectures with off-center excitation can yield stable bumps, at least in a simplified one-dimensional continuum model (Rubin and Troy, 2004).

In all of these models, the spread of activity is halted by an accumulation of inhibition at some distance from the core of the active region. In Drover and Ermentrout (2003) and Rubin and Bose (2004), however, examples of bumps in purely excitatory networks of type II and type I cells, respectively, are presented. The phenomenon of bumps in an excitatory network differs from the frequency effects discussed in Section 3, in that the introduction of excitation here

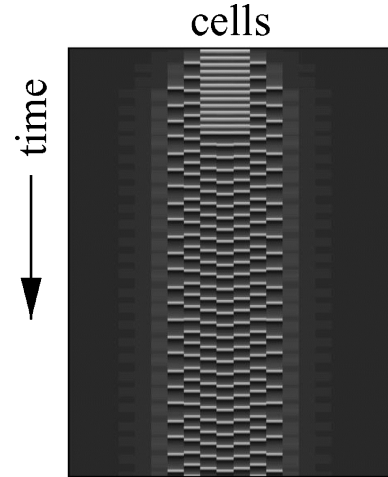


Figure 5. Sustained, localized activity in a network of 20 cells governed by (6). The greyscale encodes levels of v , with elevated v , corresponding to the active phase, represented by pale shades. A stimulus is applied to the central three cells for a brief period, causing them to fire at relatively high frequency, and is then removed; despite its removal, activity persists in the recruited subset of cells.

increases the overall activity in the network, relative to the uncoupled state. Nonetheless, given the past emphasis on Mexican hat coupling as a feature of bump-supporting networks, and more generally on inhibition for stemming the spread of activity, the fact that synaptic excitation can recruit and maintain the activity of some intrinsically silent cells in a network and yet not recruit others, despite uniform coupling architecture and strength across the network, represents a surprise.

Figure 5 shows an example of a computational experiment, similar to those in Rubin and Bose (2004), in which a bump is formed by a transient stimulation, and persists after the end of the stimulation period, in an excitatory network of 20 cells. The equations simulated, again in XPPAUT (CVODE with time step 0.01 units), are the Morris and Lecar (1981), Rinzel and Ermentrout (1998) system

$$\begin{aligned}
 v_i' &= f(v_i, w_i) - \bar{g}_{\text{syn}}[v_i - v_{\text{syn}}] \\
 &\quad \times [c_0 s_i + \sum_{j=1}^{j=3} c_j (s_{i-j} + s_{i+j})] \\
 w_i' &= [\omega_{\infty}(v_i) - w_i] / \tau_w(v_i) \\
 s_i' &= a[1 - s_i]H(v_i - v_{\theta}) - bs_i H(v_{\theta} - v_i)
 \end{aligned}
 \tag{6}$$

for $i = 1 \dots 20$, where $H(x)$ is the Heaviside step function and $s_k = s_{k+20}$ for $k < 1$, $s_k = s_{k-20}$ for $k > 20$; see Rubin and Bose (2004) for complete details. Parameters $c_0 = 0.02$, $c_1 = 0.022$, $c_2 = 0.006$,

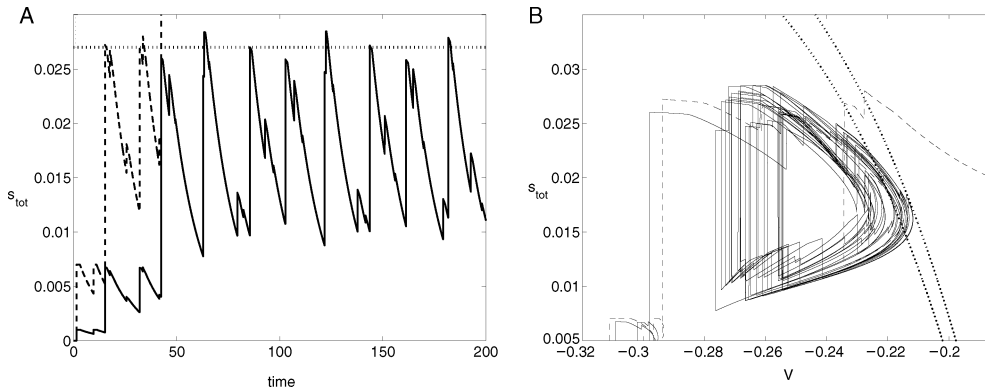


Figure 6. Inputs of similar sizes may or may not recruit a cell, depending on their timing. (A) The cell corresponding to the dashed time course is recruited by an input of magnitude $s_{\text{tot}} \approx 0.027$, marked by the dotted line. Although s_{tot} for the cell with the solid time course exceeds this level several times, the cell is not recruited. (B) Trajectories of a recruited cell (dashed) and its non-recruited neighbor (solid), under the dynamics of (6), are projected into the (v, s_{tot}) plane. The leftmost dotted curve is the cross-section of the go surface for the recruited cell that is relevant when it gets recruited. The rightmost dotted curve is a cross-section of the go surface for the non-recruited cell, which corresponds to the onset of decay for a particular input the cell received; most cross-sections relevant for other inputs lie in a small neighborhood of this one. Note that the non-recruited cell's trajectory approaches very close to the recruitment threshold but does not cross it. Both panels are reproduced, with slight modification, from Rubin and Bose (2004) with the permission of IOP Publishing Limited.

and $c_3 = 0.001$ scale the synaptic coupling to depend on distance. Note from system (6) that cells are self-coupled ($c_0 \neq 0$). While a cell with self-coupling but no other inputs will return to rest after stimulation, this self-coupling does make it easier to maintain activity than to recruit new cells. Thus, the main question in the analysis of these bumps is: what allows for the recruitment of some cells, but not others? A subtle point that arises is that the timing of inputs, not just their magnitudes, determines recruitment, as shown in Fig. 6A. The key to understanding the bump formation shown here is to note that in it, synaptic excitation acts in three different ways:

- it promotes recruitment during the stimulation period, since stimulated cells fire at high frequencies, leading to accumulation of synaptic excitation to sufficient levels to recruit non-stimulated cells within some neighborhood of the active region (depending on coupling strength, time constants, and so on);
- it prevents recruitment of additional cells by desynchronizing active cells after the stimulation period, such that inactive cells never receive sufficient input to fire; and,
- it maintains the firing of active cells after the stimulation period, since even with self-coupling, cells cannot fire persistently when decoupled from the network.

In fact, desynchronization contributes to this last effect as well, together with slow decay of excitation, by ensuring that there are no periods when all synaptic inputs to an active cell have decayed away. Given the crucial role of desynchronization in localizing and sustaining activity, the mechanism for bumps here clearly depends on the fact that the neurons in the network are type I cells, which are driven to an asynchronous state by excitation (Ermentrout, 1996); the bumps in the type II cells in Drover and Ermentrout (2003) must therefore result from a different mechanism, which remains to be fully elucidated.

The analysis in Rubin and Bose (2004) provides a framework that can be used to determine precisely which input is responsible for recruiting an activated cell. The idea is to consider the equations for a potential recruit, cell i , at a moment when the voltage of the cell itself, as well as the voltages of all of the cells that provide it with synaptic input, satisfy $v < v_\theta$. Let $s_{\text{tot}i} = \bar{g}_{\text{syn}}[c_0 s_i + \sum_{j=1}^{j=3} c(s_{i-j} + s_{i+j})]$. The relevant equations then become

$$\begin{aligned} v'_i &= f(v_i, w_i) - s_{\text{tot}i} [v_i - v_{\text{syn}}] \\ w'_i &= [\omega_\infty(v_i) - w_i] / \tau_w(v_i) \\ s'_{\text{tot}i} &= -b s_{\text{tot}i}, \end{aligned} \quad (7)$$

which have exactly three critical points, namely a stable node $(v_l, w_l, 0)$ and unstable equilibria $(v_m, w_m, 0)$

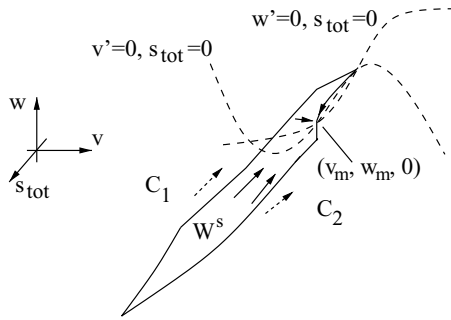


Figure 7. An illustration of the go surface (\mathcal{W}^s , solid). Under the flow of (7), trajectories evolve toward $\{s_{\text{tot}} = 0\}$, as suggested by the arrows; nullclines for $s_{\text{tot}} = 0$ are dashed, as are arrows for trajectories off of \mathcal{W}^s . The stable manifold \mathcal{W}^s of $(v_m, w_m, 0)$ partitions trajectories of (7) into those that can enter the active phase (in \mathcal{C}_2) and those that cannot (in \mathcal{C}_1). Adapted from Rubin and Bose (2004) with the permission of IOP Publishing Limited.

and $(v_u, w_u, 0)$, with $v_l < v_m < v_u$. The critical point $(v_m, w_m, 0)$ has a two-dimensional stable manifold \mathcal{W}^s that separates $\{(v, w, s) \in \mathbb{R}^3 : w < w_u\}$ into two disconnected components. One component, call it \mathcal{C}_1 , consists of trajectories that converge directly to $(v_l, w_l, 0)$ without entering the vicinity of the right branch of the v -nullcline, while the other, call it \mathcal{C}_2 , consists of trajectories that do enter this active phase before converging to $(v_l, w_l, 0)$. See Fig. 7.

Suppose that the trajectory of the potential recruit, cell i , lies in \mathcal{C}_1 and that it gets a synaptic input, say from cell j . Because cell j is active, (v_i, w_i) evolve according to the full system (6) until the moment, say t_j , when v_j falls below v_θ . At time t_j , assuming that no other presynaptic cells have fired in the meantime, system (7) becomes relevant, and we check whether $(v_i(t_j), w_i(t_j), s_{\text{tot}_i}(t_j))$ lies in \mathcal{C}_1 or \mathcal{C}_2 . In the former case, since \mathcal{W}^s is invariant (and $w' < 0$ at $w = w_u$ in \mathcal{C}_1), $(v_i(t), w_i(t), s_{\text{tot}_i}(t))$ remains in \mathcal{C}_1 until a future input to cell i arrives. In the latter case, again since \mathcal{W}^s is invariant and since any future inputs will be excitatory, it is guaranteed that cell i will fire, even if it receives no future inputs. Thus, we refer to \mathcal{W}^s as the *go surface*.

Note that, due to the curvature of \mathcal{W}^s induced by the dynamics of (7), different points with the same value of s_{tot} may lie in different \mathcal{C}_i , depending on their v and w components. Thus, the total input s_{tot} needed for recruitment is different in different cells, as in Fig. 6A, and is also different for the same cell at different times. Further, the level of s_{tot} itself differs over different inputs to the same cell, as is also ap-

parent in Figs. 6A and B. Given $(v_i(t_j), w_i(t_j), s_{\text{tot}}(t_j))$ as above, whether recruitment occurs or not can be checked in the (v, s_{tot}) plane by comparing the location of $(v_i(t_j), w_i(t_j), s_{\text{tot}}(t_j))$ to the cross-section of \mathcal{W}^s taken at $w = w_i(t_j)$, as in Fig. 6B.

Because recruitment depends so strongly on the abrupt threshold formed by \mathcal{W}^s , the localized activity in this network is sensitive to noise and to small variations in parameters. It remains possible that short-term dynamics can add robustness to this network; see Rubin and Bose (2004) for a discussion of the impact of short-term depression on the network. Alternatively, it is possible that while inhibition is clearly not a necessary ingredient for the existence of stable bumps in this type of network, inhibition plays a key role in preserving localized activity patterns in noisy conditions. Finally, spatial heterogeneity in coupling may contribute to the pinning of bumps in certain preferred locations in an excitatory network, as discussed for other coupling architectures in Renart et al. (2003) and Rubin and Troy (2004), which would be expected to enhance the robustness of the selected patterns.

5. Conclusion

The effects of synaptic excitation on a model neuronal network depend on the intrinsic dynamics of cells in the network as well as the strength and temporal characteristics of the synaptic signal. Under the right conditions, some specialized and some general, synaptic excitation can speed up, slow down, synchronize, or desynchronize network activity, and it can propagate activity throughout a network or sustain activity in a localized subregion within a network.

Acknowledgment

I thank Martin Wechselberger for comments that helped improve the clarity of this paper.

References

Abbott LF, Regehr WG (2004) Synaptic computation. *Nature* 431: 796–803.
 Amari S (1977) Dynamics of pattern formation in lateral—inhibition type neural fields. *Biol. Cybern.* 27: 77–87.
 Baer SM, Erneux T, Rinzel J (1989) The slow passage through a Hopf bifurcation: Delay, memory effects, and resonance. *SIAM J. Appl. Math.* 49: 55–71.
 Butera RJ, Rinzel J, Smith JC (1999) Models of respiratory rhythm

- generation in the pre-Bötzinger complex. II. Populations of coupled pacemaker neurons. *J. Neurophysiol.* 81: 398–415.
- Diener M (1984) The canard unchained or how fast/slow dynamical systems bifurcate. *Math. Intell.* 6(3): 38–49.
- Drover JD, Ermentrout B (2003) Nonlinear coupling near a degenerate Hopf (Bautin) bifurcation. *SIAM J. Appl. Math.* 63: 1627–1647.
- Drover J, Rubin J, Su J, Ermentrout B (2005) Analysis of a canard mechanism by which excitatory synaptic coupling can synchronize neurons at low firing frequencies. *SIAM J. Appl. Math.* 65: 65–92.
- Ermentrout B (1996) Type I membranes, phase resetting curves, and synchrony. *Neural Comput.* 8: 979–1001.
- Ermentrout B (2002) *Simulating, Analyzing, and Animating Dynamical Systems: A Guide to XPPAUT for Researchers and Students.* SIAM, Philadelphia.
- Hansel D, Mato G, Meunier C (1993) Phase dynamics for weakly coupled Hodgkin-Huxley neurons. *Europhys. Lett.* 23: 367.
- Hansel D, Mato G, Meunier C (1995) Synchrony in excitatory neural networks. *Neural Comput.* 7: 307–337.
- Hodgkin AL, Huxley AF (1952) A quantitative description of the membrane current and its application to conduction and excitation in nerves. *J. Physiol (Lond.)* 117: 500–544.
- Hoppensteadt FC, Izhikevich EM (1997) *Weakly Connected Neural Networks.* Springer-Verlag, New York, NY.
- Izhikevich E (2000). Subcritical elliptic bursting of Bautin type. *SIAM J. Appl. Math.* 60: 503–535.
- Kopell N, Somers D (1995) Anti-phase solutions in relaxation oscillators coupled through excitatory interactions. *J. Math. Biol.* 33: 261–280.
- Kuske R, Baer S (2002) Asymptotic analysis of noise sensitivity in a neuronal burster. *Bull. Math. Biol.* 64: 447–481.
- Morris C, Lecar H (1981) Voltage oscillations in the barnacle giant muscle fiber. *Biophys. J.* 35: 193–213.
- Neishtadt AI (1987) On delayed stability loss under dynamical bifurcations I. *J. Diff. Eqn.* 23: 1385–1390.
- Neishtadt AI (1988) On delayed stability loss under dynamical bifurcations II. *J. Diff. Eqn.* 24: 171–176.
- Renart A, Song P, Wang X-J (2003) Robust spatial working memory through homeostatic synaptic scaling in heterogeneous cortical networks. *Neuron* 38: 473–485.
- Rinzel J (1985) Excitation dynamics: Insights from simplified membrane models. *Fed. Proc.* 44: 2944–2946.
- Rinzel J (1987) A formal classification of bursting mechanisms in excitable systems. In: AM Gleason, ed. *Proceedings of the International Congress of Mathematicians.* AMS, Providence, RI, pp. 1578–1593.
- Rinzel J, Ermentrout GB (1998) Analysis of neural excitability and oscillations. In: C Koch, I Segev, eds. *Methods in Neuronal Modeling: From Ions to Networks,* second edition. MIT Press, Cambridge, MA, pp. 251–291.
- Rubin J, Bose A (2004) Localized activity patterns in excitatory neuronal networks. *Network: Comp. Neural Sys.* 15: 133–158.
- Rubin J, Terman D (2002) Geometric singular perturbation analysis of neuronal dynamics. In: B. Fiedler, ed. *Handbook of Dynamical Systems,* Vol. 2 Elsevier, Amsterdam, pp. 93–146.
- Rubin J, Terman D, Chow C (2001) Localized bumps of activity sustained by inhibition in a two-layer thalamic network. *J. Comp. Neurosci.* 10: 313–331.
- Rubin JE, Troy WC (2004) Sustained spatial patterns of activity in neuronal populations without recurrent excitation. *SIAM J. Appl. Math.* 64: 1609–1635.
- Somers D, Kopell N (1993) Rapid synchronization through fast threshold modulation. *Biol. Cybern.* 68: 393–407.
- Su J, Rubin J, Terman D (2004) Effects of noise on elliptic bursters. *Nonlinearity* 17: 133–157.
- Szmolyan P, Wechselberger M (2001) Canards in \mathbb{R}^3 . *J. Diff. Eqn.* 177: 419–453.
- Wang X-J, Rinzel J (1995) Oscillatory and bursting properties of neurons. In: MA Arbib, ed. *Handbook of Brain Theory and Neural Networks.* MIT Press, Cambridge, MA, pp. 689–691.
- Wechselberger M (2004) Existence and bifurcation of canards in \mathbb{R}^3 in the case of a folded node. Preprint.
- Wilson HR, Cowan JD (1973) A mathematical theory of the functional dynamics of cortical and thalamic nervous tissue. *Kybernetik* 13: 55–80.